Biophysical Journal, Volume *117*

Supplemental Information

Surface and Bulk Stresses Drive Morphological Changes in Fibrous Microtissues

Erik Mailand, Bin Li, Jeroen Eyckmans, Nikolaos Bouklas, and Mahmut Selman Sakar

Supplementary Figures

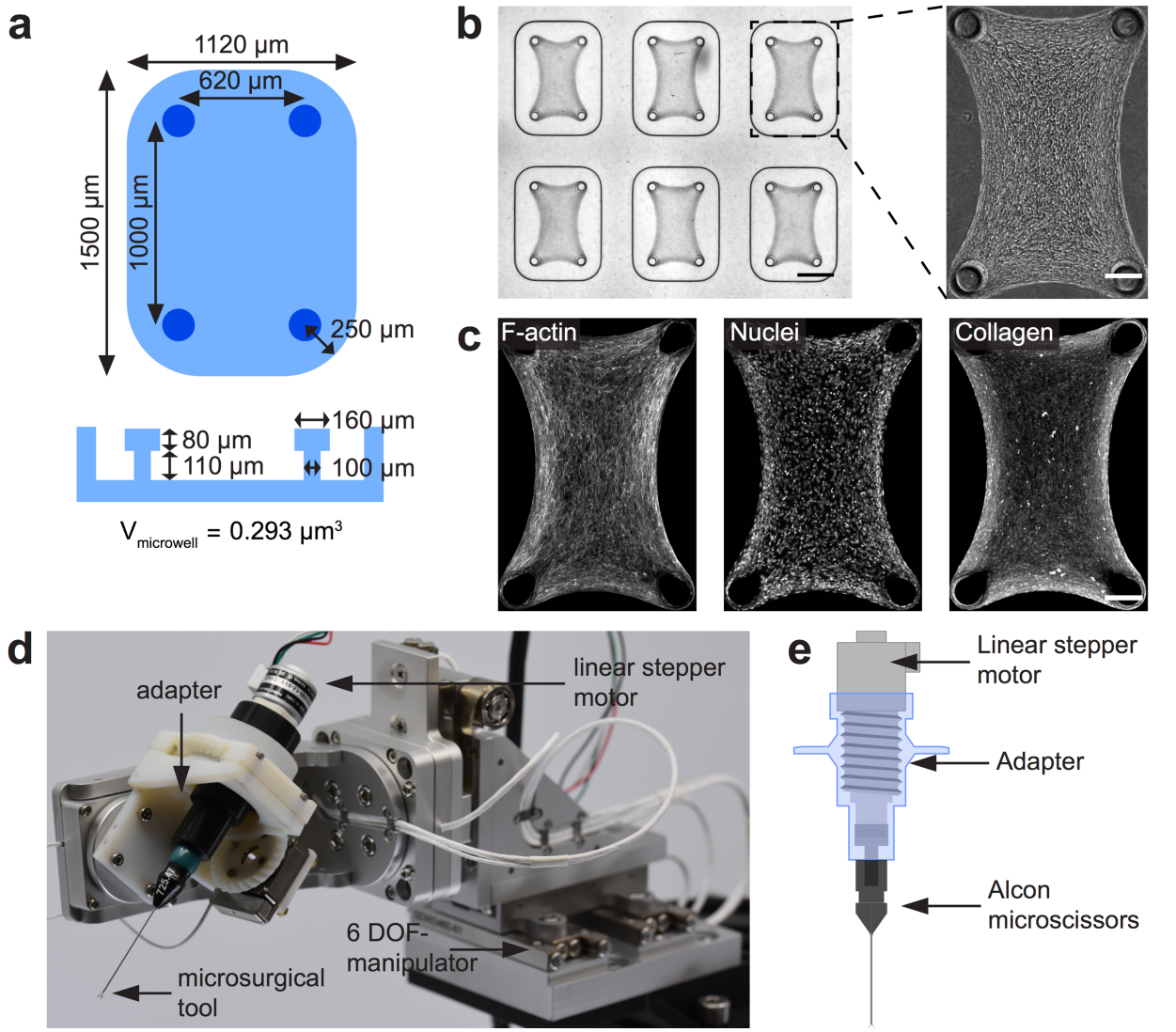

Figure S1. Experimental platform. The operator observes the microtissue using an inverted microscope and telemanipulates the end-effector of the instrument with a 5-DOF joystick. (a) Schematic showing the dimensions of microwells and cantilevers. (b) Phase-contrast image of an array of engineered fibrous microtissues and the close-up view of a single construct. Scale bars, 500 µm and 150 µm. (c) Confocal micrographs of a representative microtissue stained with Phalloidin (F-actin), Hoechst (nuclei), and anti-collagen Alexa-647 (collagen fibres). Scale bar, 150 µm. (d) Photograph of the 6-DOF robotic micromanipulation system. (e) Section view of the 3D-printed adapter along with a disposable surgical instrument actuated by a linear stepper motor.

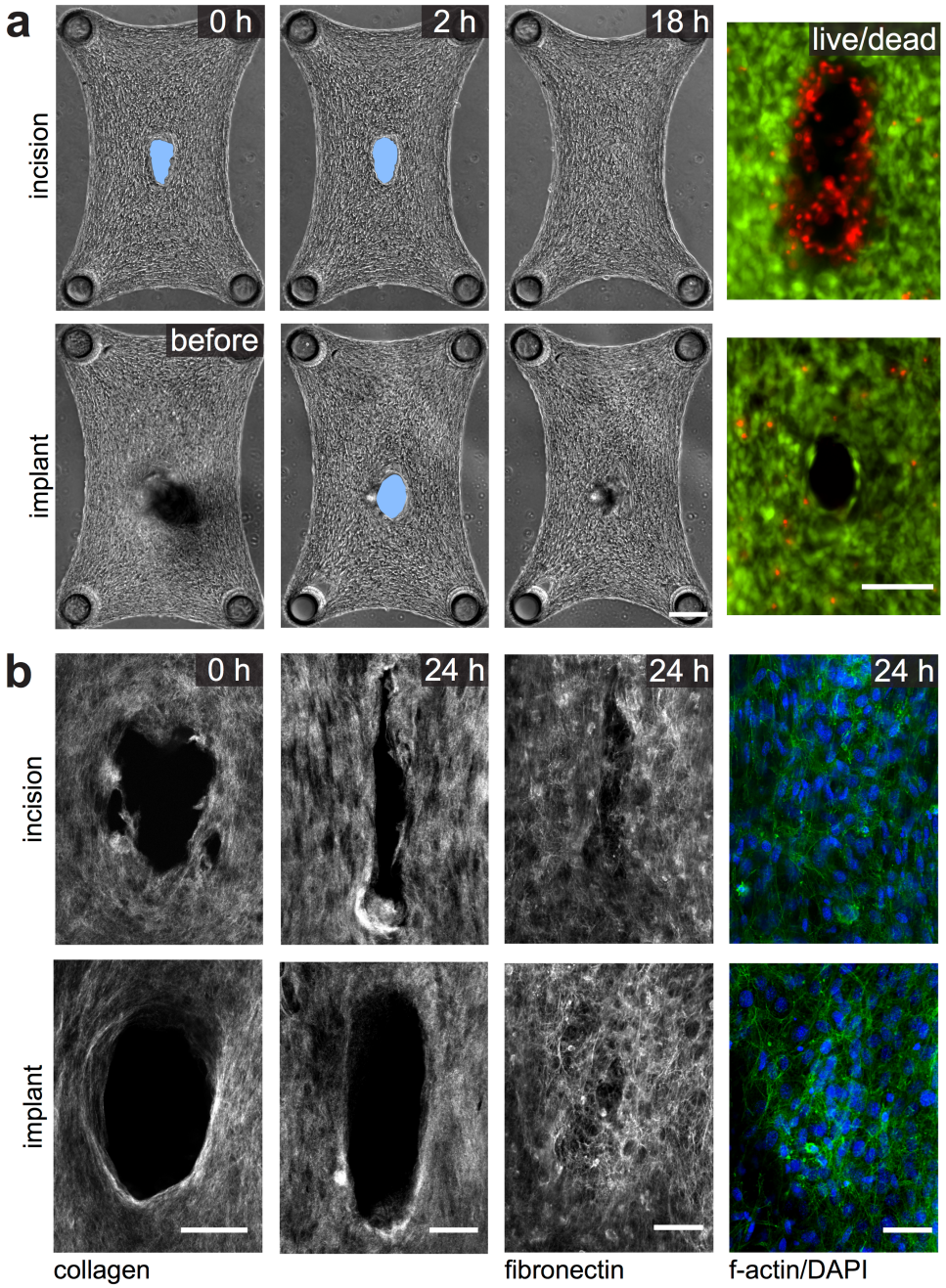

Figure S2. Closure of incision wounds and damage-free holes. (a) Upper panel: Micrographs showing the closure of wounds introduced by microsurgical incision. Live/dead staining of the wound area right after incision. Lower panel: Micrographs showing the closure of damage-free holes introduced by the removal of an implant. Live/dead staining of the gap right after the formation of the hole. Scale bars, 150 µm and 100 µm respectively. (b) Two-photon and confocal images of the wound area. Collagen fibres were visualized with second harmonic imaging microscopy. The tissues were stained for fibronectin, f-actin, and nuclei. Scale bars, 50 µm.

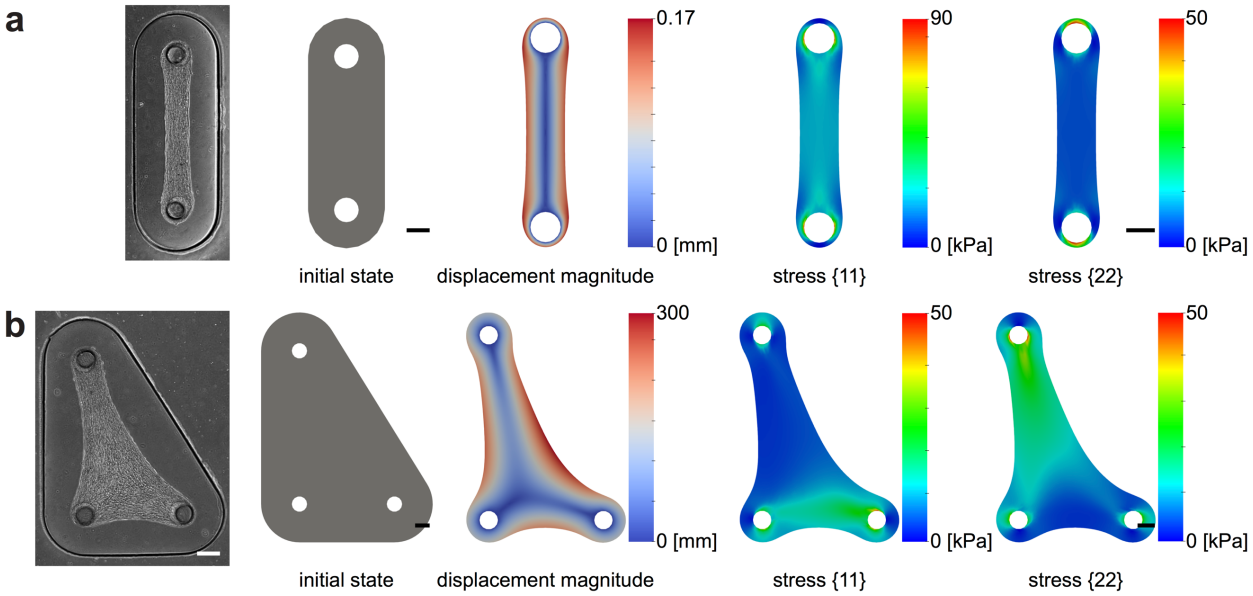

Figure S3. Finite element simulation of microtissues with different geometries. A representative phase-contrast image of the engineered microtissues is shown along with the displacement magnitude (left) and stress maps (right) for (a) two-post and (b) three-post configurations. Scale bars, 150 μm.

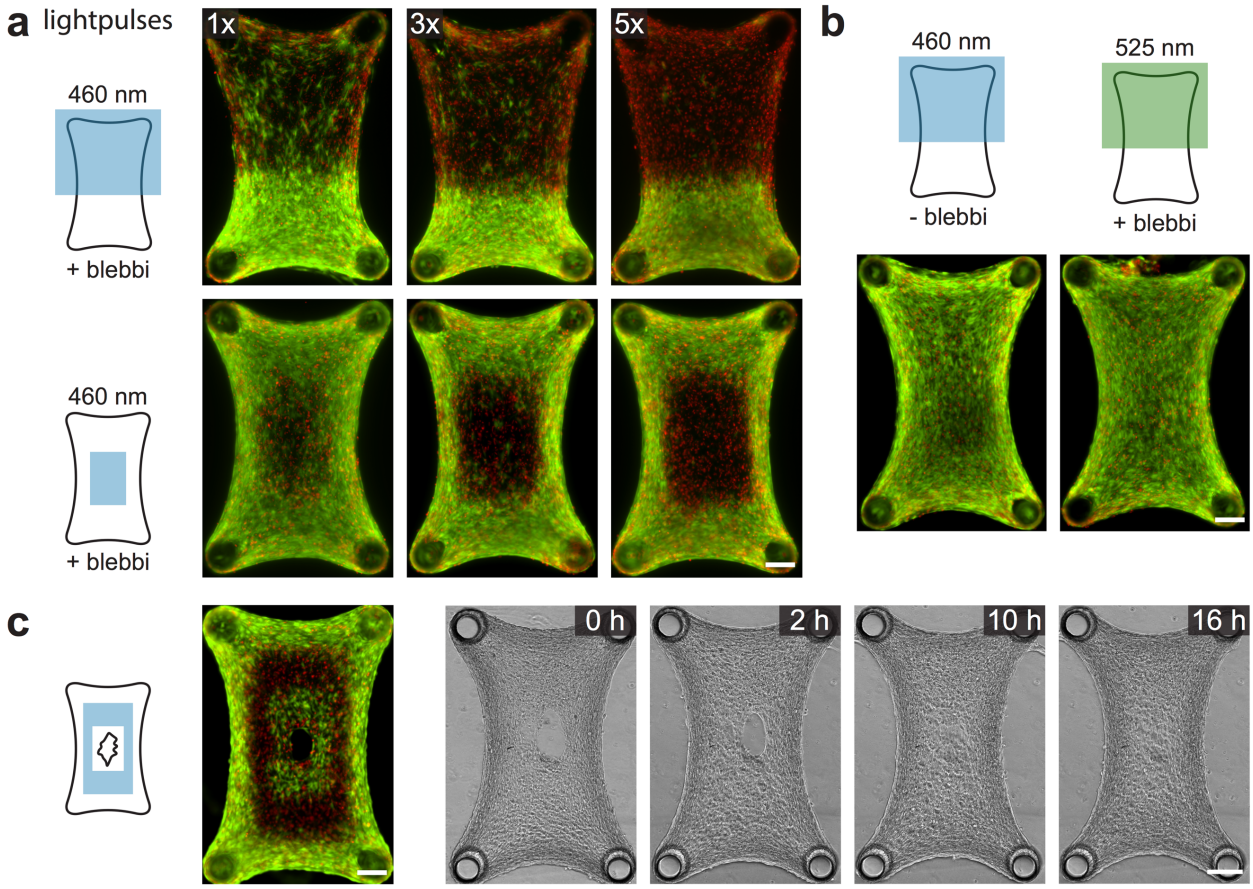

Figure S4. Spatiotemporally controlled photoconversion of blebbistatin and cell death in microtissues. The efficacy of treatment is assessed with live/dead staining (live, green and dead, red). (a) Optimization of the exposure protocol. Pulses of blue light (460 nm) exposure is generated for 3 seconds. A 30 second break is given in between consecutive pulses. Five pulses are enough to ensure complete killing within the targeted area. Half of the tissue (upper panel) or the center of the tissue (lower panel) is targeted to show that the treatment does not depend on the location. (b) Blue light exposure in the absence of blebbistatin or green light (525 nm) exposure of blebbistatin show no phototoxic effect on the exposed area. The treatment requires the presence of the chemical and is wavelength specific. (c) Live/dead staining and temporal sequence of micrographs of microtissues that is treated in region 2 (between the wound edge and the outline). Scale bars, 150 µm.

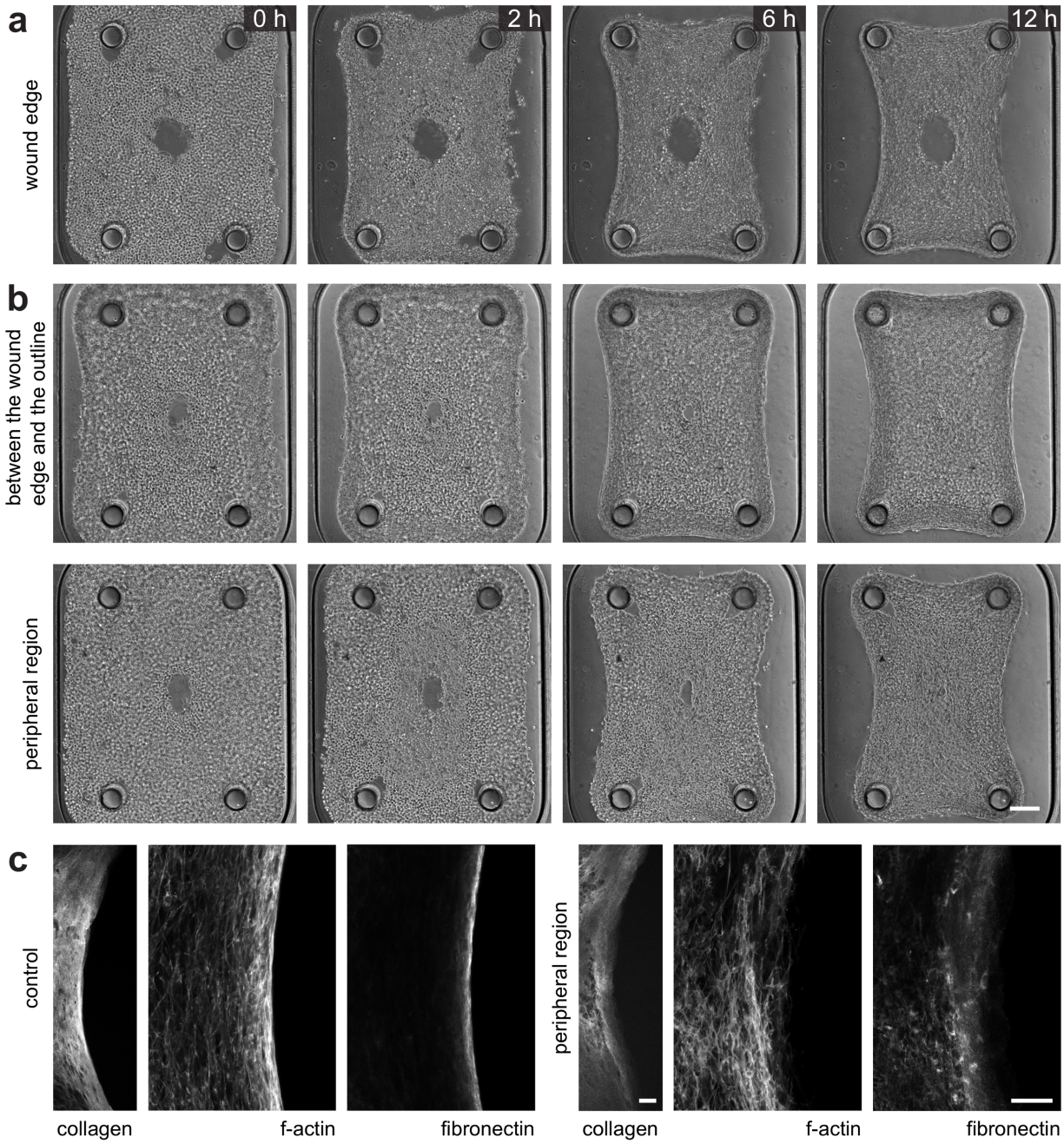

Figure S5. Deactivation of surface effects during tissue formation. Temporal sequence of micrographs showing the morphological changes after illumination at the (a) wound edge and (b) the region between the wound edge and the outline or the tissue periphery. Medium containing 20 μM blebbistatin was added to the culture medium 30 minutes after seeding the cell/collagen suspension. Scale bar, 150 μm. (c) Confocal sections showing collagen, F-actin, and fibronectin at the periphery of the microtissues with and without exposure at the periphery. Images are taken 14 hours after tissue formation. Scale bar, 50 μm.

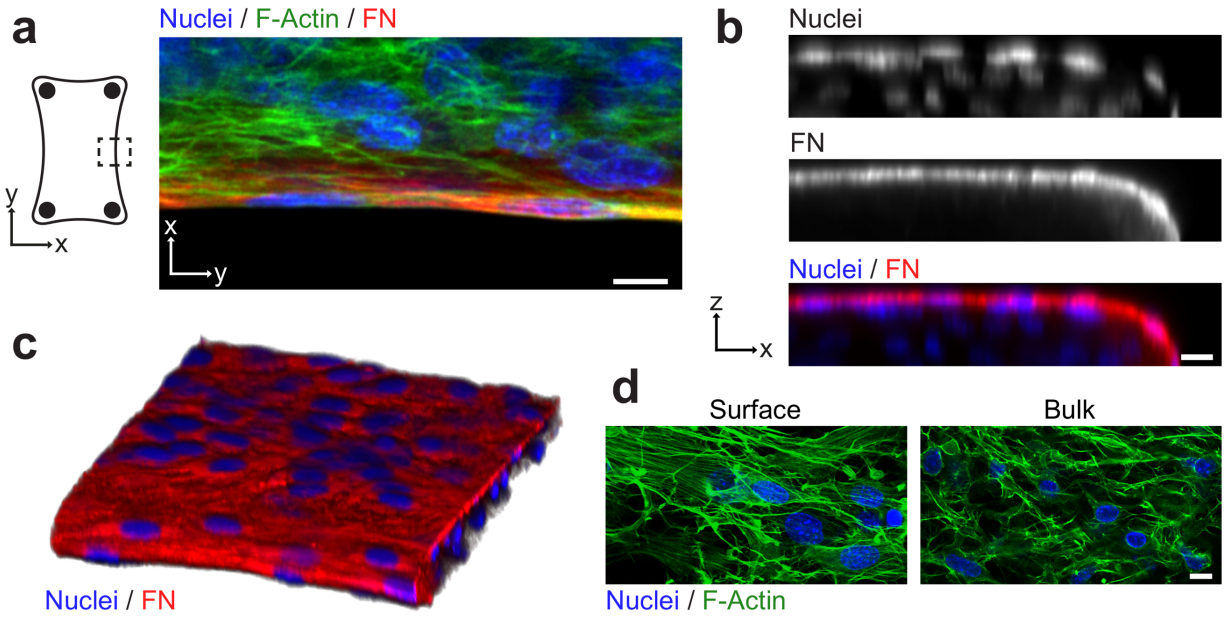

Figure S6. Tissue architecture suggests the presence of surface stresses. (a) Immunofluorescence optical section of the boundary shows aligned elongated cells embedded in a fibronectin rich matrix at the tissue periphery. (b) Cross-sectional view of a representative microtissue shows a gradient of fibronectin. (c) 3D reconstruction of confocal slices shows higher levels of fibronectin at the tissue periphery and smooth edges at the side. (d) Optical sections show different cytoskeletal architecture at the surface compared to cells in the bulk of a microtissue. Presence of stress fibers is an indication of higher stresses. Scale bars, 10 µm.

Supplementary Movies

Movie S1. Robotic micromanipulation platform.

Movie S2. Formation of microtissues.

Movie S3. Compaction and reshaping of microtissues prior to release from the cantilevers.

Movie S4. Closure of closed-contour wounds and gaps.

Movie S5. Spatially controlled phototoxic treatment.

Movie S6. Shape restoration after open-contour incisions.